Chemical Engineering Journal 486 (2024) 150036

Contents lists available at ScienceDirect

Chemical Engineering Journal

journal homepage: www.elsevier.com/locate/cej

Triggering triboelectric nanogenerator antibacterial Activities: Effect of charge polarity and host material correlation

Marziyeh Jannesari [a,b,1,*], Faezeh Ejehi [c,1], Niall J. English [a], Raheleh Mohammadpour [b], Omid Akhavan [b,d], Soroush Shams [e]

[a] School of Chemical and Bioprocess Engineering, University College Dublin, Belfield, D04 V1W8 Dublin, Ireland
[b] Center for Nanoscience and Nanotechnology, Institute for Convergence Science & Technology, Sharif University of Technology, 14588- 89694 Tehran, Iran
[c] Department of Materials and Metallurgical Engineering, Amirkabir University of Technology, P. O. Box 1591634311, Tehran, Iran
[d] Department of Physics, Sharif University of Technology, P.O. Box 11155-9161, Tehran, Iran
[e] School of Chemical Engineering, College of Engineering, Tehran University, 16th Azar St., Enghelab Sq., P. O. Box 11155-4563, Tehran, Iran

ARTICLE INFO

Keywords:
Triboelectric nanogenerator (TENG)
Graphene oxide (GO)
Antibacterial properties
Reactive oxygen species (ROS)
Electrical stimulation (ES)
Electron transport chain (ETC)

ABSTRACT

Triboelectric nanogenerators (TENGs) offer promising motion-driven energy harvesting for human–machine interactions, particularly in wearable healthcare and biomedical devices. However, direct skin contact demands addressing aggressive bacterial growth risks. The "triangle" interaction between bacteria, electrical stimulation, and host materials has been investigated comprehensively in the present study to facilitate appropriate self-antibacterial designs for TENGs. In so doing, it was revealed that the growth of negatively charged bacterial models (*Escherichia coli* and *Staphylococcus aureus*) was inhibited by induced positively charged substrates (Al or graphene oxide (GO)), regardless of the host material's composition due to the direct electrostatic interactions. Electron capture from the bacterial respiratory chain by the substrates leads to the interruption of the bacterial energy supply. In response to negative charges, however, an appreciable host-dependent antibacterial behaviour was observed, with Al showing a negligible bactericidal effect, while GO exhibited robust antibacterial properties. This effect was assigned to reactive oxygen species (ROS) generation, triggered by shuttling the negative charges to the oxygen functional groups in GO, suppressing bacterial growth efficaciously. The observed correlation between the electrostatic charge polarity and the material composition of the substrates (hosting the bacteria) highlights the superiority of ROS induction in the antibacterial properties of TENG. These findings pave the way for developing innovative approaches to control bacterial growth effectively and enhance the applicability of TENGs as advanced wearable devices with inherent antibacterial capabilities.

1. Introduction

According to the World Health Organization (WHO), pathogenic bacterial infections are regarded as one of the primary contributors to mortality [1]. Of greater significance is the established correlation between bacterial infections, which are progressively becoming more dangerous, and the onset of various life-threatening diseases such as cancer [2], osteomyelitis [3] and septic arthritis [4]. The substantial and continuous rise in drug resistance among bacterial strains, primarily caused by the misuse and/or overutilization of antibiotics in both livestock and human healthcare, has led to notable global concern [5]. These challenges have resulted in additional economic and public health burdens, leading to a growing demand for the development of novel antibacterial treatments. Therefore, growing interest has been developing in introducing innovative approaches to combat bacterial infections [6] and addressing the challenges associated with the rising concern of drug-resistant bacteria. There has been a notable stream of interest in utilizing physical strategies including electrical stimulation (ES) (using electrical currents to activate specific nerves or muscles in the body) for controlling and/or combating pathogenic bacteria, while simultaneously minimizing potential side effects to circumvent drug-resistance restrictions [7,8].

Among others, very recently, triboelectric nanogenerators (TENGs) as a highly promising technology for their remarkable capability of

* Corresponding author.
E-mail address: marziyeh.jannesari@ucd.ie (M. Jannesari).
[1] These authors have contributed equally to this work.

https://doi.org/10.1016/j.cej.2024.150036
Received 29 November 2023; Received in revised form 20 February 2024; Accepted 26 February 2024
Available online 28 February 2024

electrical energy harvesting (from mechanical motion and associated friction) demonstrated potential for antibacterial activities [9–11]. Apart from the advantages such as low cost, variable design, and consistent performance repeatability, TENGs with self-power capability eliminate the necessity for external power sources, thereby enhancing their practicality and sustainability [12,13]. Moreover, the flexibility of TENGs enables them to adapt seamlessly to the movements of the human body, making them highly versatile for wearable applications [14,15]. However, prolonged direct contact with the skin, required for continuous energy harvesting, may promote conditions favourable for aggressive bacterial growth. As a result, there has been a high demand for incorporating antibacterial activity into the TENG devices to facilitate their application in various biomedical devices. Several studies have been conducted to explore methods of imparting antibacterial capabilities. The main approach involves loading antibacterial components, such as Ag nanoparticles [16], and a combination of TiO_2 and Ag [17], into the TENG electrodes. In addition, some TENGs exploit the inherent antibacterial nature of the electrodes, such as bromobutyl rubber (BIIR) [18,19], to help prevent bacterial growth. Very recently, researchers have investigated the role of electrostatic interactions between the opposite surface charges of bacteria and the TENG electrodes [20], disrupting the bacterial respiratory chain to inhibit bacterial growth [9].

Despite continuous research efforts, a significant lack of information persists regarding the combination and importance of the above-mentioned mechanisms, which are still poorly understood. To gain a more comprehensive understanding of the fundamental mechanisms and their implications for bacterial physiology, additional investigations are warranted. Bearing this in mind, this study aims to explore the integrity, significance, and synergistic and correlative effects associated with the disruption of the bacterial respiration chain and the induction of oxidative stress, specifically focusing on the influence of the electrode nature.

To accomplish this goal, two materials, graphene oxide (GO) and aluminum (Al) were selected as the surfaces to host bacteria. Graphene-based materials as two-dimensional carbon nanostructures, characterized by their single-layer atom thickness, have garnered significant interest across various research domains [21]. With remarkable physicochemical properties, including a large surface area [22,23] and high electron mobility [24], graphene nanostructures have found utility across diverse research domains, including biomedical applications [25], photocatalysts [26], and as promoters for nanobubble generation [27]. However, oxygen functional groups along with structural defects in GO restrict its application in devices requiring electrical conductivity due to the charge transfer constraints [28]. Introducing Al foil with high electrical conductivity as a back layer can address this restriction by facilitating the charge transfer to the GO electrodes. Furthermore, the flexibility and lightweight characteristics, coupled with the affordability and stability of Al [29], render it particularly suitable for wearable TENGs, meeting the essential requirement for adaptability to diverse surfaces. Moreover, considering the widespread use of Al foils in food packaging, the potential to introduce antibacterial properties through spontaneous mechanical motion further enhances its utility.

In this study, both sides of GO and Al serving as the host substances, received electrical charges from the TENG electrodes to investigate how the electrode nature and the ES can collaboratively integrate to establish antibacterial effects. To experience charges with different polarities, the prepared host (GO/Al) electrode was electrically connected to the single-electrode TENG (S-TENG) (either the GO or Kapton both on Al), tapped with a Kapton- or latex-wrapped finger, respectively. The results showed that an interplay between bacteria, the polarity of electrical stimulation, and host materials can determine the optimum design for antibacterial properties in TENG systems. Indeed, positively charged hosts inhibited bacterial growth through electrostatic interactions (between the substrates with positively charged and bacteria with negatively charged surfaces), while negatively charged substrates, particularly graphene oxide, effectively suppress bacteria by generating reactive oxygen species (ROS). This study can provide opportunities for pioneering approaches to regulate bacterial growth, thus improving the suitability of TENGs in cutting-edge wearable devices.

2. Results and discussion

2.1. Material characterization

Morphological studies via atomic force microscopy (AFM) technique (Fig. 1A) confirm the formation of monolayer GO nanosheet with a thickness of ~ 0.8 nm [30–32]. The X-ray diffraction (XRD) pattern of the GO nanosheets in Fig. 1B displays a prominent and intense (0 0 2) peak at ~ 10.8°, suggesting the successful exfoliation of carbon sheets compared to the primary graphite powder (~26.7°) [32]. These findings are in line with the UV–Vis absorption spectrum of the GO sheets (Fig. 1C), where the peak at ~ 230 nm corresponds to the π-π* transitions (a signature of the C–C bond), and the shoulder appeared at around 310 nm can be assigned to the n-π* transition of the C = O bond [33].

Drop-casting of GO suspension on Al foil produced a layer with a remarkably thin thickness of only ~ 7.44 μm (cf. Fig. 2A). The flexibility of the prepared GO layer on Al facilitates opportunities for various applications, wearable sensors, and biomedical nanogenerators. The cross-sectional field emission scanning electron microscopy (FE-SEM) image of GO depicts a layered structure formed during the environmental drying process. Simultaneously, a slight shift was observed (from ~ 10.8° to ~ 12.3°) in the peak of the XRD pattern for the dried GO film (Fig. 2B). This can be attributed to the desorption of water molecules among the exfoliated GO sheets, as well as the trivial restacking phenomenon [32,34]. The maintenance of this separated and dispersed state is desirable for various applications that rely on the unique properties of GO. In addition, Raman-spectroscopy analysis shown in Fig. 2C revealed the presence of characteristic D and G bands of GO sheets at 1350 cm^{-1} and 1594 cm^{-1}, indicating the defects and sp^2 carbon bonding in graphene oxide respectively [34]. This observation provides further confirmation of the presence of individual GO sheets in the GO layer on the Al foil. Fourier-transform infrared (FTIR) characteristic peaks (Fig. 2D) at around 1243, 1627 and 3429 cm^{-1} assigned to C-O-C, C = O and OH functional groups, which further validate the unchanged chemical structures of GO after drop casting.

2.2. TENG output studies

The triboelectric performance of the prepared electrodes was investigated through finger tapping in a vertical contact-separation mode. Due to its higher electron affinity (according to the triboelectric series), negative charges are generated on Kapton upon tapping, while concurrently producing positive charges on the surfaces of latex or GO in both presented TENG setups (Fig. 3A). The reciprocating motion of the upper layer generates an alternating current, reflecting the reciprocating motion of electrons during each tapping cycle to maintain equilibrium within the TENG setup. Notably, this current exhibits significantly higher values in one direction (Fig. 3B). The electrical stimulation, predominantly occurring during the release phase of each tapping cycle (Fig. S1) and distinguished by notable spikes in the current diagrams (denoted as $I_{release}$ opposite to the current direction) is considered as the primary ES ("charge") in this work for simplification purposes. To further illustration, for inducing positive or negative charges on the incubated bacteria, the TENG electrodes made of either GO/Al or Kapton/Al were electrically connected to the GO or Al host substrates through a wire, as shown in Fig. 3. Subsequently, the TENG electrodes were tapped with a Kapton-wrapped or latex-covered finger, respectively. Finger tapping (~3 Hz) on GO/Al or Kapton/Al electrodes exhibited average output currents of 16.6 ± 3.2 and -19.6 ± 4.0 μA and average voltages of 169 ± 19 and -258 ± 34 V, respectively.

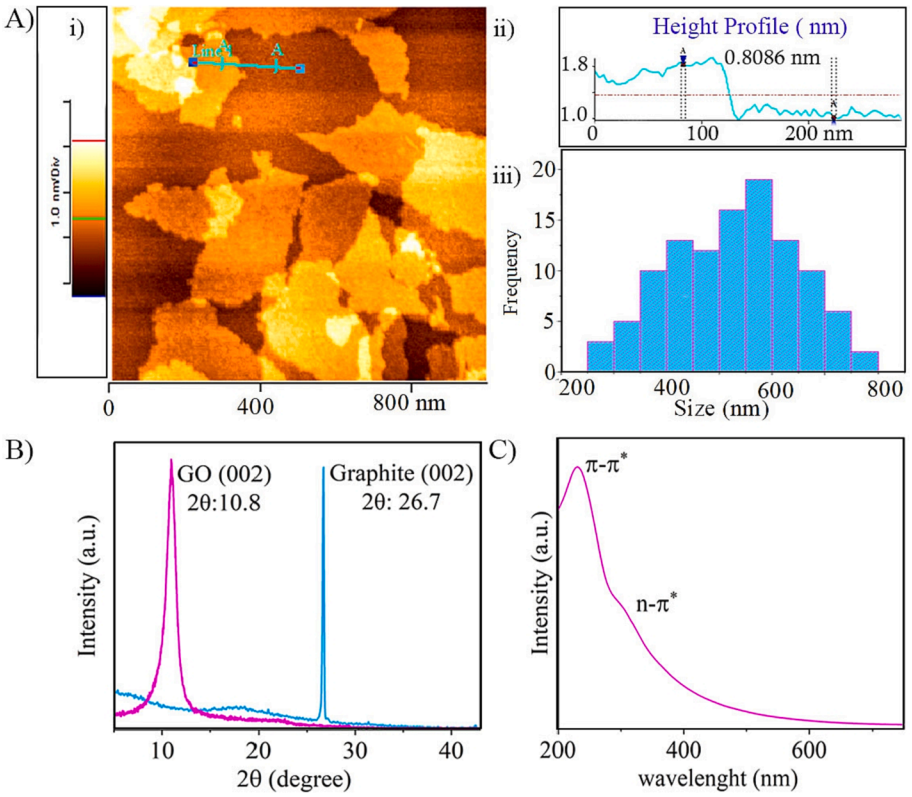

Fig. 1. Analysis of the chemically synthesized GO suspension. (A) atomic force microscopy (AFM) investigation of GO: (i) image, (ii) the height profile of one randomly selected sheet of GO indicated with the blue line, and (iii) lateral size distribution of the GO sheets. (B) XRD patterns comparing GO nanosheets (pink) to its precursor, graphite powder (blue), (C) UV–Vis absorption spectrum of GO nanosheets suspension. (For interpretation of the references to colour in this figure legend, the reader is referred to the web version of this article.)

2.3. Simulation results

Mirroring the manually triggered ES (cf. Fig. 3A), the external electric field in the non-equilibrium molecular-dynamics simulations was applied both in the upper and lower direction, to induce polarisation across the interfacial GO-Al system. Here, the Hirshfeld charges [35] were computed after 5 ps of system relaxation, and the field-induced shift in the atomic charges was $\sim 0.034 \pm 0.012$ e in magnitude; this leads to substantial scope for ES-induced electron transfer between the GO-Al layers and TENG (*vide infra*).

2.4. Antibacterial studies

The antibacterial properties of the host electrodes under TENG-based electrical stimulation (ES) were investigated and compared with those of the electrodes not subjected to electrical stimulation. These tests were conducted in the mid-log phase characterized by exponentially rapid cell division and multiplication at which the bacteria are metabolically active. This phase with a swift rate of bacterial growth provides a larger population for assessing the impact of the antibacterial agent. Consequently, the significance lies in controlling bacterial proliferation during the early stages to proactively curb their growth [36]. To capture the immediate responses of bacterial models to ES, a brief 10-minute timeframe was chosen. In contrast, to investigate the more lasting effects of TENG-based electrical stimulation, an extended period of 25 min was opted, providing a more comprehensive understanding of the sustained impact on bacterial activity. Two main approaches including optical density (OD_{620}) measurements as well as colony-forming unit counting were used to study the antibacterial behaviours of the treatments.

Generally, the amount of light capable of passing through a growth medium, containing bacteria reversely indicates the concentration of the bacteria in the solution. In fact, in this investigation, the higher the concentration of the bacteria, the less the transparency of the liquid will be recorded. Therefore, the optical density of a sample at a special wavelength (620 nm) can be considered as an indicator (OD_{620}) for bactericidal growth promotion or inhibition.

As demonstrated in Fig. 4, in the absence of ES, Al as the host electrode did not, by its very nature, exhibit antibacterial effects against both gram-negative and gram-positive bacterial models. However, when a positively charged finger-tapping-based electrical current was stimulated, a slight "aggression" can be observed in the Al-incubated bacteria. On the other hand, negatively charged Al shows negligible bactericidal effects on both bacterial models.

In contrast, when exposed to GO, bacteria experienced destructive effects even in the absence of ES. Furthermore, these effects were remarkably enhanced upon receiving stimulated electrical charges - especially when the exposure time to electrical induction increased from 10 to 25 min. Interestingly, bacteria exhibited an inverse charge-dependent response upon replacing Al with GO: when loaded with negative charges, GO exhibited more efficient bactericidal effects against both bacterial models as compared to the positively charged ones.

The number of colony-forming units obtained from either treated and untreated bacterial cells exhibits a similar trend as observed in OD_{620} measurements. Results indicated that, regardless of TENG-based electrical stimulation, the Al side was not effective in inhibiting bacterial growth. However, when the bacteria were exposed to the GO side, bactericidal activity was significantly enhanced especially upon exposure to finger-tapping-induced electrical stimulation. Therefore, this reconfirms that beyond the electrode nature, the polarity of the induced electrical charges on the host electrode can effectively control bacterial

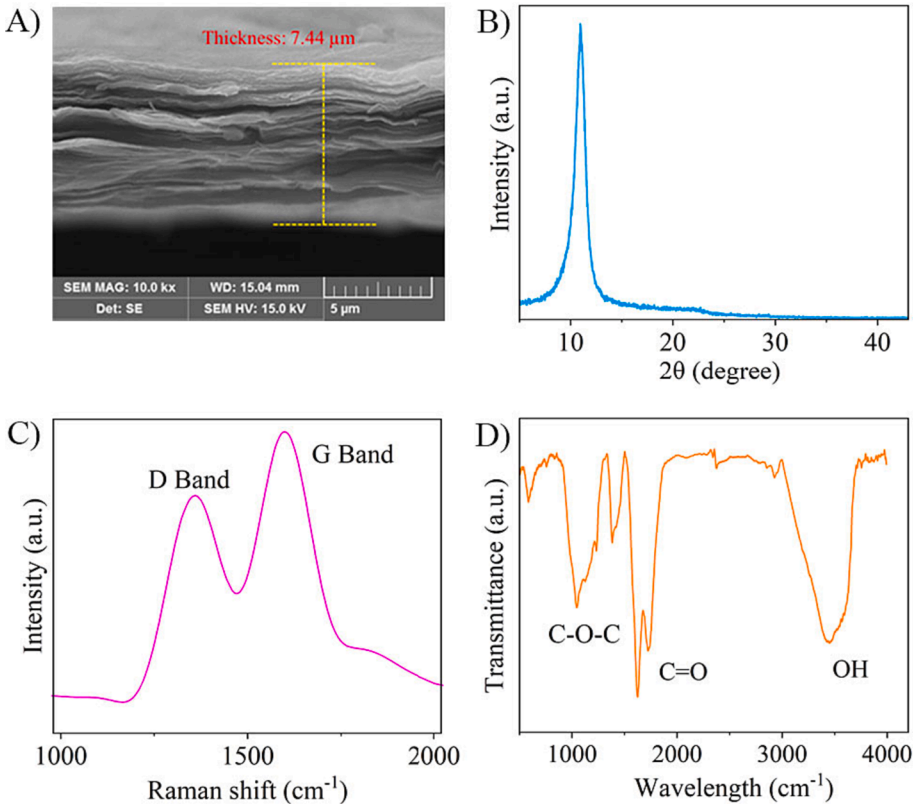

Fig. 2. (A) Cross-sectional FE-SEM image, (B) XRD pattern, (C) Raman and (D) FTIR spectra of the prepared GO film on Al foil. These analyses confirm minimal restacking of GO layers, attributed to water desorption between the layers, thereby preserving the distinctive properties of GO sheets within the resulting film.

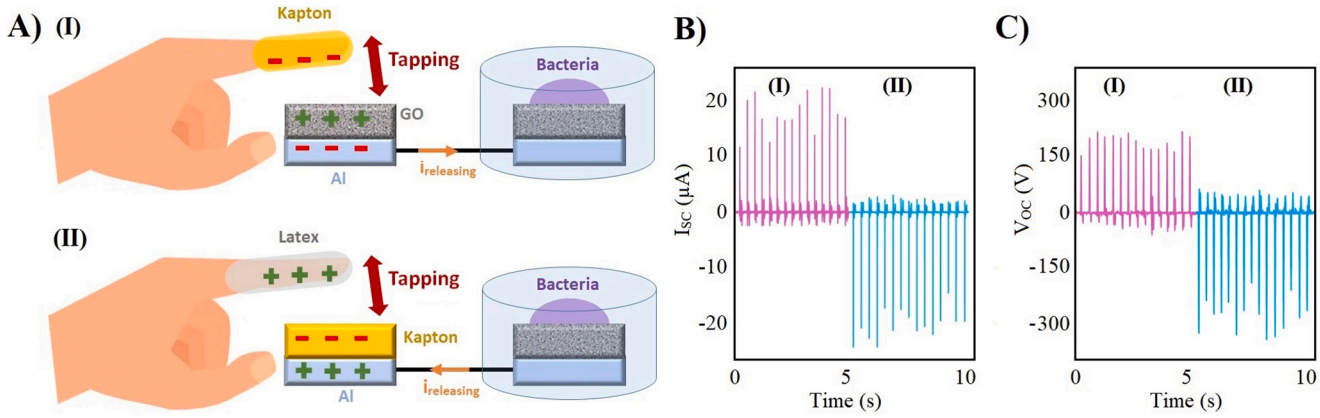

Fig. 3. (A) Schematic illustration of finger-tapping-based TENGs of Kapton on GO (I) and latex on Kapton (II), inducing positive and negative charges on the host substrates during the releasing state, respectively. Output signals of (B) short circuit current and (C) open-circuit voltage from the mentioned TENGs. The size of the electrodes was 2 × 2 cm^2, the frequency and the approximate height of tapping were approximately 3 and 5 cm, respectively.

growth. Fig. 4 illustrates that bacteria exposed to a negatively charged-induced GO layer underwent severe destructive responses, resulting in significantly fewer bacterial populations, especially with longer exposure times (25 min). These results highlight the role of the induced charge type on the host electrodes in bacterial inactivation.

A critical question arising here is whether the observed antibacterial properties originated from just the inherent antibacterial properties of GO nanosheets [37], or whether TENG-based electrical stimulation can also augment this behaviour. To address this critical question, the bacterial cells on the host electrodes were kept incubated overnight by adding molten agar to the electrodes without further electrical stimulation. As illustrated in Fig. S2, the growth of bacteria in contact with Al experiencing no electrical stimulation resulted in huge bacterial populations. Furthermore, subjecting Al electrodes to electrical stimulation for 10 min, irrespective of the charge polarity (positive or negative), did not significantly suppress the growth of either bacterial model when they were exposed to those electrodes for extended periods without electrical stimulation. In contrast, a noticeable distinction is observed between the bacterial growth on the GO side of the electrode without any electrical stimulation and those subjected to induced electrical effects, particularly with a negative charge. These findings serve to provide even greater clarity on the significance of electrical stimulation concerning the nature of the electrode in bactericidal performance.

To delve deeper into the influence of electrode surface properties

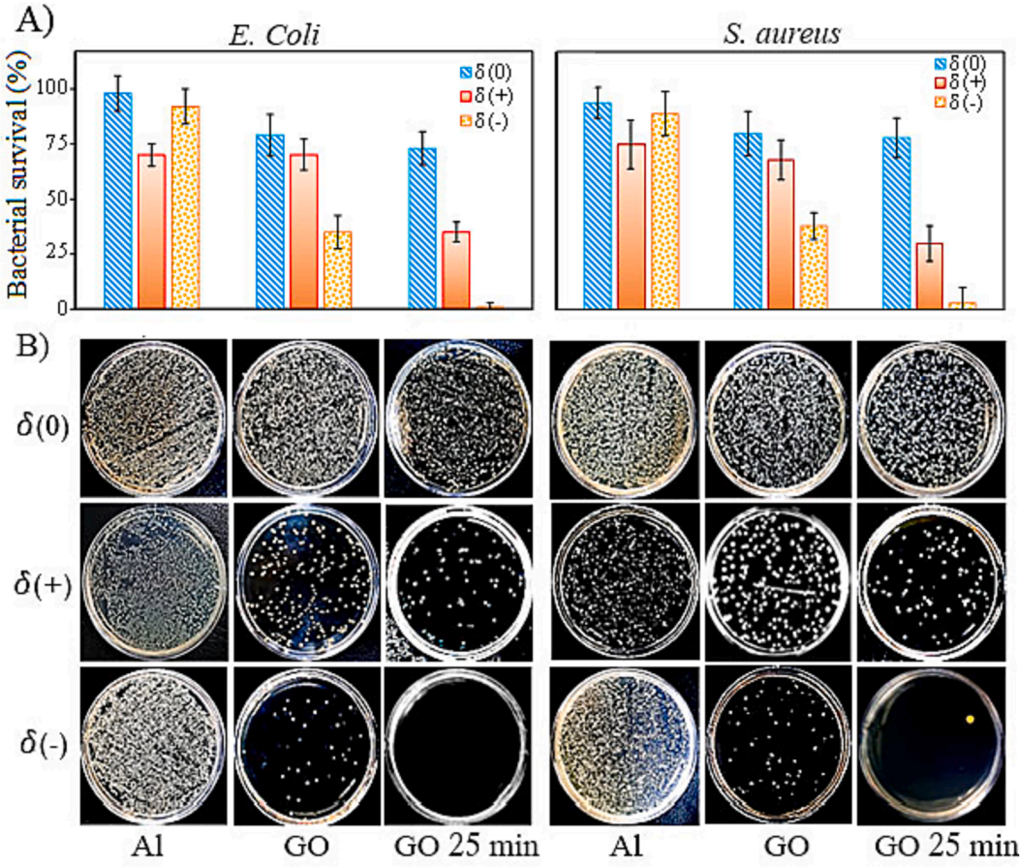

Fig. 4. Response of *E. coli* and *S. aureus* bacteria, hosted on different substrates of Al and GO to positive and negative TENG-based electrical stimulation (for 10 and 25 min), studied through (A) OD_{620} and (B) colony counting methods.

(especially water affinity) on TENG-mediated antibacterial behavior, Al electrodes were subjected to a 10-min exposure to hot DI water (~90 °C), inducing a transition from hydrophobic to hydrophilic surfaces. The results revealed a substantial increase in the hydrophilicity of the Al surfaces, as evidenced by a remarkable reduction in the water droplet contact angles from ~ 92 to 11° (Fig. S3). This phenomenon can be attributed to the formation of grass-like nanostructures [38], of Al_2O_3 grown on the surface of Al foil as confirmed by X-ray photoelectron spectroscopy (XPS) in Fig. S4. Significantly, unlike the untreated Al electrodes, the hydrophilic Al, enriched with oxygen functional groups via hot (DI) treatment for 10 min, demonstrated pronounced antibacterial properties upon exposure to TENG-based electrical stimulation (refer to Figures S5 and S6). This observed behavior indicates a strong correlation between surface hydrophilicity and the elicited antibacterial response. Specifically, hot water-treated (HWT) Al electrodes demonstrated a notable enhancement in their antibacterial efficacy, an effect that was further augmented with prolonged exposure to electrical stimulation (from 10 to 25 min). Moreover, the results reveal analogous antibacterial trends between HWT Al surfaces and GO electrodes under TENG stimulations.

While the classical colony-counting method is a valuable approach for assessing the bactericidal properties of a treatment, there are restrictions in its ability to distinguish between deactivated and dead cells. Even though deactivated live cells may not be able to form colony units, they can be revived under certain conditions. Several techniques, such as the live/dead staining method using specific fluorescent dyes, have been used to reveal the latency life of deactivated bacteria for distinguishing between live and dead cells [39]. To further investigate the viability of bacterial cells, a fluorescent staining approach, utilizing acridine orange/propidium iodide (AO/PI) was employed. The AO probe can penetrate both intact and damaged cell membranes and stains them green, while the PI probe can only enter cells with damaged membranes and reacts with DNA to emit red fluorescence. Hence, this method enables differentiation between live (green) and dead (red) bacterial cells [39,40].

2.5. Live/Dead bacterial staining study

As depicted in Fig. 5, in the absence of electrical stimulation (ES), the Al host was found to even support the growth of both bacterial models, as evidenced by emitting highly intensified green fluorescence (indicating live bacteria), without any red fluorescence (representative for dead bacteria). Accordingly, Al can be considered as bacterial-friendly under these conditions. Similar results were obtained when the Al carried negative charges. However, when positive charges were stimulated to the Al host electrode, the red fluorescence (indicative of dead bacteria) emerged, while the green emission from the live bacteria decreased. The GO electrodes, however, exhibited inherent antibacterial properties in the absence of electrical stimulation, as evidenced by the presence of red-stained (damaged) bacteria in addition to green-emitting (live) bacteria. The intensity of the red emission was enhanced when the GO electrode was positively charged (by discharging electrons towards the bottom electrode to maintain the charge balance). Simultaneously, with a decrease in green fluorescence, the intensity of red fluorescence significantly increased upon shuttling the electrons into the GO electrodes, inducing negative charges. Interestingly, a remarkable enhancement in the red emission was observed when the bacterial cells on the GO electrodes were subjected to electrical stimulation for a longer period (up to 25 min). These findings reconfirm the synergistic effect of the inherent properties of GO and the electrical stimulation in antibacterial activities.

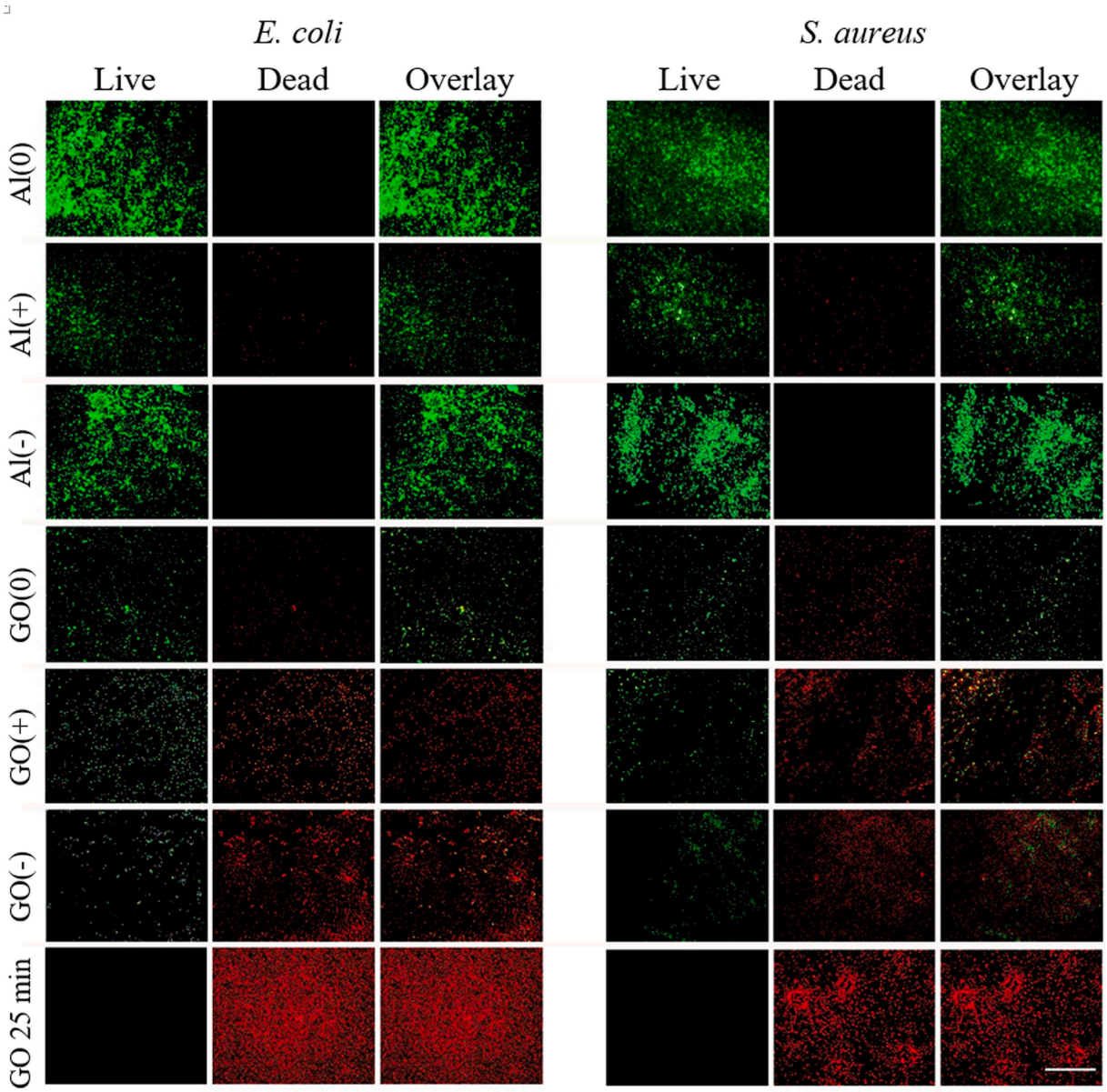

Fig. 5. Live/dead fluorescent staining images of the bacterial models of *E. coli* and *S. aureus,* exposed to different host substrates of Al and GO, loaded with positive and negative TENG-based electrical stimulation for 10 and 25 min. The scale bar is representative of 100 μm.

2.6. Morphological investigations of the bacteria by FE-SEM analyzing

To gain deeper insight into the antibacterial properties of the electrodes and their impact on bacterial membranes under TENG-based electrical stimulation, FE-SEM imaging was employed to visualize the structural changes in bacteria. Fig. 6 illustrates the responses of both *E. coli* and *S. aureus* bacteria to the positively charged Al side of the host electrode, where a slight shrinkage in the bacterial membrane was observed, indicating a subtle enhancement of the antibacterial activity. However, when the charge polarity of the Al host electrode changed to negative, their smooth shapes and distinct membrane boundaries remained intact. Importantly, no signs of collapse or rupture were detected in the FE-SEM imaging, further supporting the notion of minor antibacterial behaviour by negatively charged Al electrodes.

In contrast, regardless of the charge polarity, both bacterial models on GO exhibited significant structural deformation when treated with TENG-based electrical effect. The bacterial membranes displayed rough and blurry surfaces, with clear evidence of perforation and rupture formation on their cellular membranes upon exposure to the GO under the influence of TENG-based electrostatic charge exposure. Notably, besides the electrical stimulation effect, the presence of GO nanosheets with sharp edges, acting as "nano-knives", as it were – which effectively support the bactericidal activities. From the polarity charge perspective, the negatively charged treated bacteria underwent more pronounced morphological deformation, validating their superior antibacterial efficiency. Ultimately, a comprehensive deformation with disintegrated membranes appeared by increasing the exposure time to the charged GO side.

2.7. Antibacterial mechanism study

To elucidate the mechanism(s) underlying the observed antibacterial properties, the extent of reactive oxygen species (ROS) generation (as one major reported antibacterial mechanism) under different treatments was qualitatively and quantitatively examined. A qualitative investigation was conducted by detecting green fluorescent light emitted from the oxidized form of non-fluorescent dichlorofluorescein-diacetate (DCFH-DA) upon reacting with intracellular ROS generated in bacterial cells

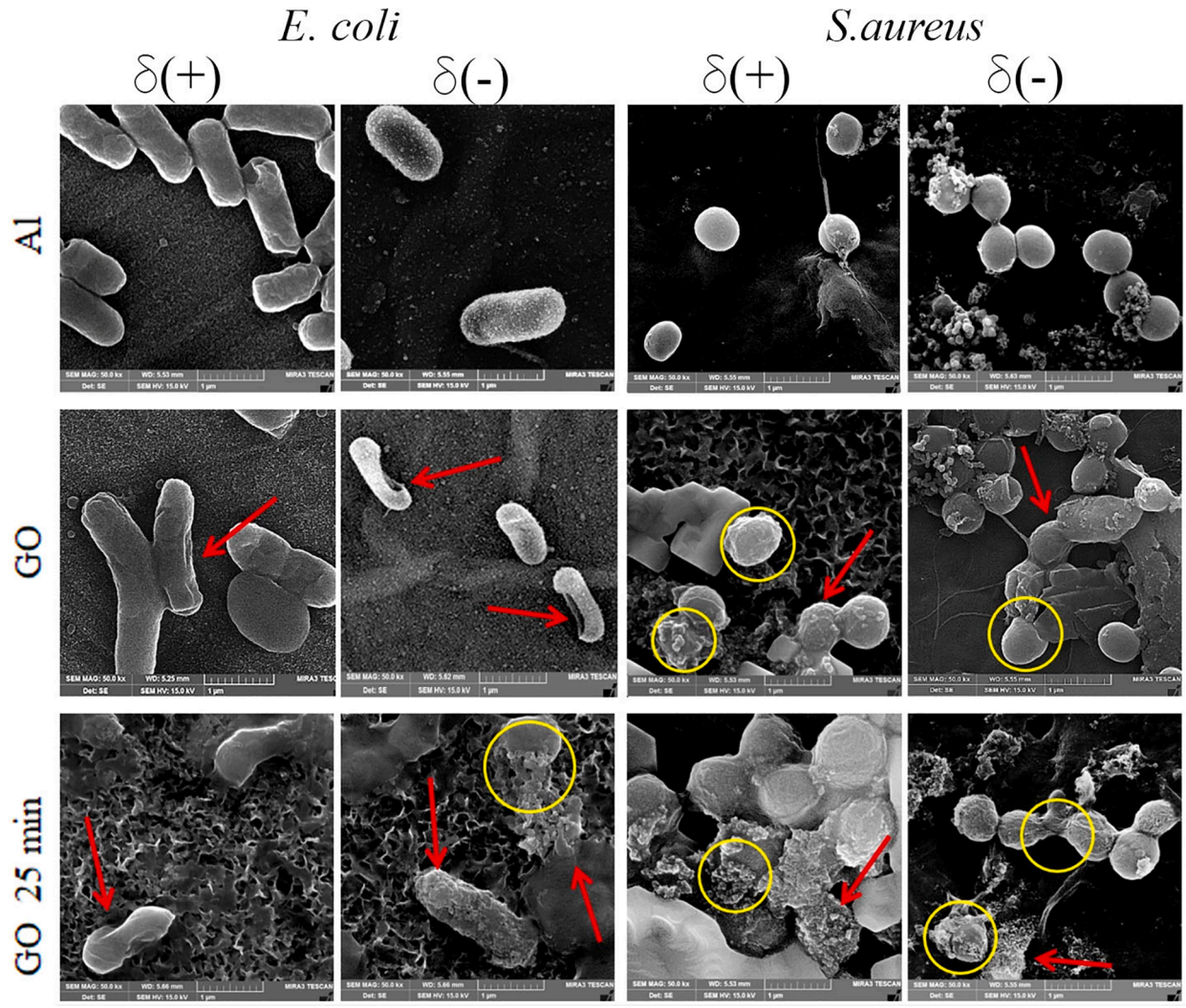

Fig. 6. Microstructure FE-SEM images of *E. coli* and *S. aureus* bacteria, incubated on Al and GO surfaces while experiencing TENG-based stimulated negative and positive charges for 10 or 25 min.

[41]. Fig. 7A depicts that negligible oxidate stress was induced on bacterial cells incubated on the Al side of the electrode, either treated with or without ES. On the other hand, a remarkable green fluorescent was radiated (representing ROS generation) from both bacterial models in contact with GO electrodes, especially when the electrodes were loaded with negative charges. This effect is significantly enhanced by increasing the ES time.

It has been established that bacteria are capable of electrically interacting with their environment through the exchange of electrons, known as extracellular electron transfer (EET) [42]. During respiration, in the electron-transport chain (ETC), electrons are shuttled in a chain from a donor to a more electronegative acceptor, providing the cells with the required energy to sustain their life [43]. This process commences from the outer membrane as the initial donor and terminates with molecular oxygen as the final acceptor, generating energy and water in reaction with hydrogen [44]. However, in the meantime, a fraction of electrons may leak and/or even be extracted from the transport chain [45,46]. While trapping electrons from the ETC can disrupt the energy-providing cycle, it can also result in transferring the trapped electrons to nearby accessible oxygen molecules, inducing ROS generation [47]. This dual effect of disturbing the ETC, as well as ROS generation, can negatively affect bacterial survival.

This response was further supported by quantitative methods on individual ROS, including the singlet oxygen ($^1O_2$) and hydroxyl radicals ($^{\cdot}OH$) generation, as demonstrated in Fig. 7B-I and 7B-II. Exposure to positively charged host substrates, both Al and GO, induced a slight production of ROS, regardless of the material. However, interactions of bacteria with negatively charged substrates displayed a material-dependent response. Indeed, while Al exhibited nearly no ROS generation, GO showed very high ROS generation. Increasing the exposure time to the ES significantly augmented the generation of both $^1O_2$ and $^{\cdot}OH$.

Both bacterial models, possessing negative surface charges, demonstrate a tendency to be absorbed onto positively charged Al and GO electrodes due to electrostatic attraction. Therefore, positively charged electrodes can interfere with bacterial respiration by extracting electrons from the ETC to maintain electrostatic balance on the host electrode [9]. This effect can disrupt the energy-generating cycle and reduce the viability of bacterial cells. Moreover, the trapped electrons can be subjected to available oxygen. Available oxygen-rich functional groups in GO (as demonstrated in FTIR spectrum in Fig. 2D) can attract the trapped electrons and induce ROS. However, negligible oxidative stress was observed from bacteria-inoculated Al electrode due to the lack of accessible oxygen molecules. Interestingly, although negatively charged GO electrodes induced the most oxidative stress on bacteria (as indicated by the high intensity of green fluorescence), negatively charged Al electrodes caused the least oxidative effect.

As anticipated, the experiments revealed that the duration of

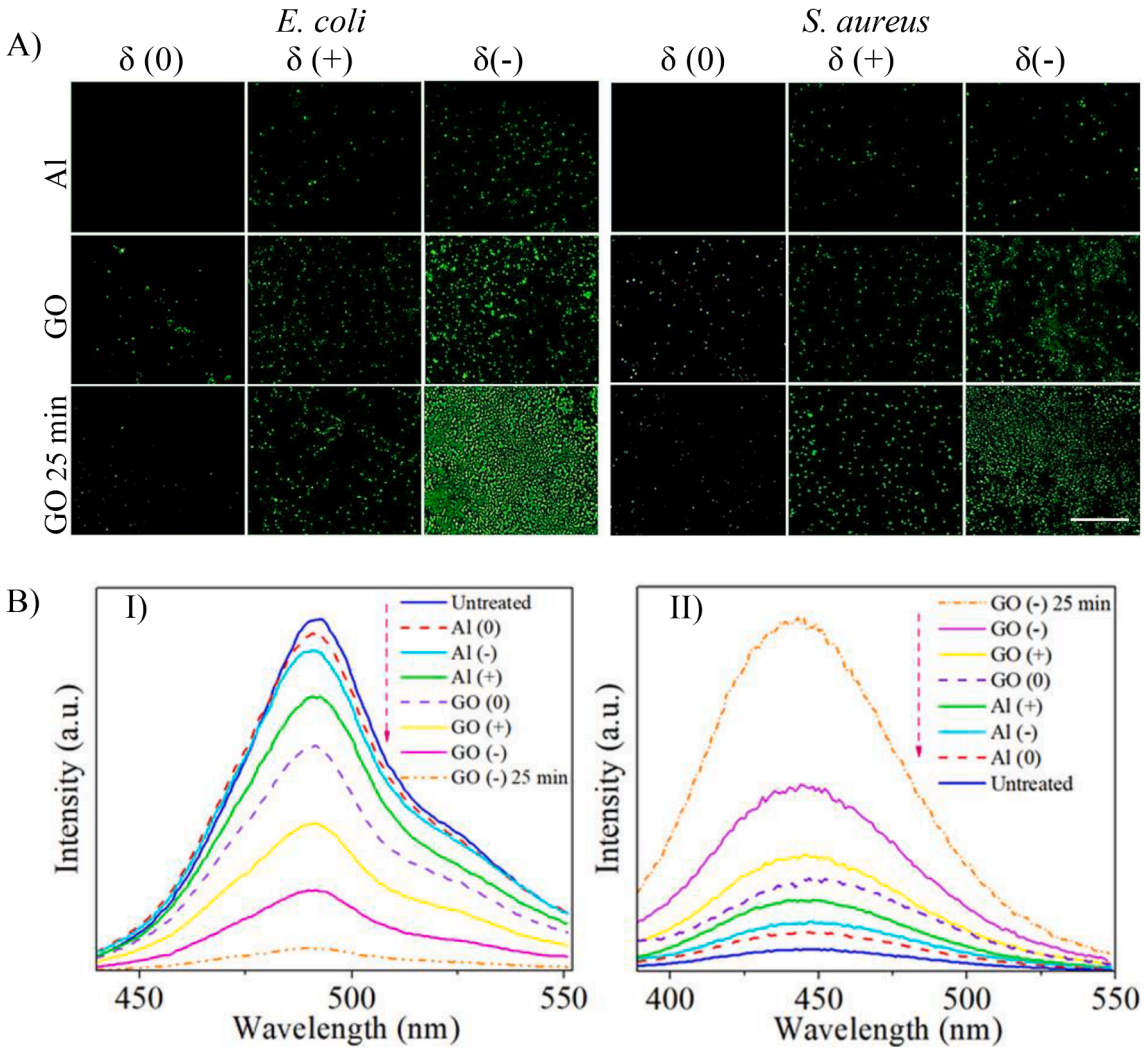

Fig. 7. (A) Qualitative (visualized by a fluorescent microscope) and (B) quantitative (measured through PL investigations) intracellular reactive oxygen species (ROS) generation in bacterial models, exposed to positively and negatively charged host substrates (Al and GO), respectively. The intensity of green fluorescent emission in (A) qualitatively indicates the level of induced ROS in bacterial cells. The generated (I) singlet oxygen ($^1O_2$) and (II) ·OH radicals shown in panel (B) were measured by molecular probes of 1,3-diphenylisobenzofuran (DPBF) and terephthalic acid (TPA) for *E. coli* bacteria, respectively. The scale bar in the picture shows a 100 μm-size. (For interpretation of the references to colour in this figure legend, the reader is referred to the web version of this article.)

electrical stimulation directly correlates with the level of reactive oxygen species (ROS) generated. With no tendency in trapping electrons from ETC to disturb bacterial respiration in negatively charged GO, the induction of oxidative stress is debatable, and can certainly be critiqued. In such circumstances, the excess number of electrons can readily meet oxygen functional groups on the surface of GO electrodes, leading to ROS production. Obviously, exposure to negative ES for a longer duration can dramatically facilitate the reaction between oxygen functional groups and the electrons on GO electrodes, causing higher levels of ROS. Quantitative studies on ROS generation also validate the trend observed in the ROS staining approach.

Analysis of intracellular ROS generation in the incubated bacteria on HWT Al electrodes experiencing the TENG-based ES (Fig. S7), exhibited heightened ROS induction when exposed to a negatively charged surface. This intriguing observation can be attributed to the surface oxygenation of Al, which promotes ROS generation in response to incoming electrons. The ROS investigation also revealed a positive correlation between exposure time and the produced ROS for the bacteria incubated on HWT Al electrodes. This behavior, influenced by changes in both hydrophilicity and surface chemical composition (from Al to oxygen-rich Al), highlights the multifaceted impact of surface modifications on antibacterial outcomes. Additionally, it accentuates the role of oxygen functional groups of the host electrodes in generating ROS when exposed to TENG operation.

To confirm further the proposed mechanism concerning the involvement of oxygen functional groups in ROS generation, a key player in the TENG-based antibacterial activities, we are considering the integration of electron paramagnetic resonance (EPR) as an alternative and precise technique in our forthcoming research.

According to these proposed mechanisms, experiencing electron deficiency, the host electrodes can electrostatically interact with bacteria with negatively charged surfaces and extract electrons from their respiratory chain, leading to bactericidal effects. Conversely, an excess number of electrons on the host electrode can be transferred to its oxygen functional groups, inducing ROS that combat bacteria effectively. Hence, both antibacterial mechanisms have potential impacts on bacterial models in each TENG cycle due to the reciprocating motion of electrons. However, as the rate of charge transfer in one direction (dQ/dt) is significantly higher, resulting in increased charge transfer (dQ) within a specific period (dt), one antibacterial mechanism prevails during each tapping cycle. This showcases the intricate interplay between these mechanisms, although fascinating, requires comprehensive investigation.

3. Conclusions

The comprehensive investigation revealed intriguing results regarding the correlative effects of TENG-based induced electrostatic charges and the host materials on bacterial models of *E. coli* and *S. aureus*. Regardless of the host material's composition, positively charged Al or graphene oxide substrates slightly suppressed the growth of negatively charged bacterial models. This effect was attributed to direct electrostatic interactions between the host substrates and bacteria, leading to the capture of electrons from the bacterial respiratory chain and disrupting the bacterial energy supply. However, when negative charges were present, a noticeable difference in antibacterial behaviour was observed depending on the host material. The Al substrate exhibited the least, whereas GO demonstrated the greatest antibacterial properties. This effect can be attributed to the induced ROS generation, which was triggered by the transfer of negative charges to the oxygen functional groups within GO, effectively inhibiting bacterial growth. The study establishes a correlation between the induced electrostatic charge polarity and the material composition of the substrates hosting the bacteria, where non-equilibrium molecular-dynamics may also be a useful "electrostatic-engineering" prototypical design tool in materials design for manipulation of ES-induced electron transfer. In any event, these studies of ES and substrate selection for optimal electron-transfer characteristics underscore their significant role in driving ROS generation and action in conferring antibacterial properties to TENGs. Indeed, mastery of such materials design for judicious electron-transfer dynamics and associated ROS-profiling is pivotal in a new era in rigorous and effective TENG-design principles.

4. Materials and methods

4.1. Graphene oxide synthesis

GO nanosheets were chemically synthesized through a straightforward modified Hummers' method from the precursor of natural graphite powder, as described in detail in Supplementary Information.

4.2. TENG electrode fabrication

In this study, 10 mL of GO suspension (5 μg/mL), synthesized via modified Hummer's method, was decanted on an Al foil inside a plastic mold and dried at ambient conditions to fabricate GO/Al host electrodes, serving as the substrate for hosting bacteria. These substrates were electrically connected to two different TENG single-electrode structures, already fabricated from Kapton or GO on Al foils. The S-TENG electrodes were then finger-tapped with Kapton or latex, to induce electrostatic charges with opposite polarities. In this design, the host electrodes functioned as the ground by facilitating the excess electron exchange inward in or outward from the main electrodes of the TENG. This "electron shuttling" can generate positive or negative electrostatic charges on the host electrode, respectively.

4.3. Computational modelling study

Non-equilibrium Density-Functional Theory in the General Gradient Approximation with the Perdew-Burke-Ernzerhof functional [48] was used in the presence of external electric fields to model the shifting of the point charges in the GO nano-sheets surface in contact with the Al layer. The applied electric field mimicked the experimental situation with the connected TENG electrodes – with the field acting in both directions (perpendicular to the interface) to mimic the negative- and positive-charging carried out experimentally. This was accomplished by using coordinates from the geometry-preparation procedure for the GO nanosheet from ref. 33 [49], whilst the Al layer was deposited thereon in three layers in the $Fm\bar{3}m$ space group; the level of interfacial strain was less than ~ 1 %. The CP2K software package was used to implement second-generation Car-Parrinello dynamics in the presence of external electric fields using the Berry-phase approach [50]: here, the time-step was 1 fs and the field intensity was 0.05 V/Å, which results in nuclear forces no more than about 1–2.5 % of those from intrinsic electric fields and is in the linear-response régime [50].

4.4. Material characterization investigation: Methodology

The morphological structures, surface topographies and size distribution of GO nanosheets were studied by analyzing their atomic-force microscopy (AFM) images using IP (2.1) image analysis software. The X-Ray diffraction (XRD) patterns of the suspension and the dried GO layer were recorded on a Philips X'pert diffractometer (utilizing a radiation source of Cu Kα, $\lambda = 1.542$ A°) with a step size of $2\theta = 0.026°$. UV–vis absorption spectrum of aqueous GO suspension was obtained by using a PerkinElmer Lambda 25 spectroscopy. The microscopic structural features of the prepared GO layer were examined using field emission scanning electron microscopy (FE-SEM) with a MIRA3, 5KV TESCAN (Brno, Czech Republic). Raman spectroscopy of the GO layer was carried out through a TakRam (N1-541, Teksan) under the 532 nm wavelength, and its Fourier-transform infrared (FTIR) spectrum was recorded over a range of 400–4000 cm^{-1} in transmission mode using an FTIR spectrometer (MBB Bommem, MB-100). A high-resolution X-ray photoelectron spectrometer (XPS), KRATOS AXIS Ultra DLD spectrometer, equipped with a monochromatic Al Ka source (1486.6 eV, 150 W), was employed for the detailed investigation of the chemical states of Al foil surfaces, thereby confirming the successful formation of oxygen functional groups on the HWT Al foil. Experiments were carried out under vacuum conditions ($<10^{-9}$ mbar) at room temperature. Subsequently, meticulous data analysis was performed, including Shirley background subtraction and Gaussian curve-fitting for peak deconvolution, enabling precise interpretation of the data and comprehensive characterization of the chemical composition and oxidation states. Ultimately, the voltage and current of the induced electricity were recorded by an oscilloscope (DSO1022A) and an Ivium Compactstat, respectively. All of the characterization investigations were performed at room temperature.

4.5. Preparation for antibacterial tests

Antibacterial behaviour of the TENG electrodes was studied on Escherichia coli (*E. coli,* ATCC® 25922™) and Staphylococcus aureus (*S. aureus*, ATCC® 25923™) bacteria (as gram positive and negative bacteria, respectively) through two main methods, including optical density measurement at 620 nm (OD_{620}) and counting the grown colony forming unit (CFU) on the plate agar.

Before the antibacterial investigations, all of the wires, glassware, and culture medium including Muller Hinton Broth (MHB, Merck), phosphate buffer saline (PBS, Merck), and agar were autoclaved at high-pressure and 120° C for 20 min for sterilization. To avoid any unexpected chemical structure changes in GO, both sides of the electrodes were sterilized by exposing them to a UV lamp for 30 min.

For the antibacterial test, as a first step, a suspension of the bacterial models with the concentration of 0.5×10^8 colony forming unit (CFU) at their mid-phase log was prepared. Subsequently, 100 μL of the bacterial suspension was carefully spread onto the surface of the host electrode (2×2 cm^2) connected to the TENG electrodes using a sterilized wire. Immediately following bacterial incubation, either a Kapton-wrapped or latex-covered finger tapping was applied to the GO or Kapton TENG electrodes to induce an electrical current (Fig. S8), respectively. Thus, the bacteria incubated on the surface of the host electrodes instantly experienced transferred electrical stimulation (ES) from the TENG electrode through the wire. After simultaneous inoculation for either 10 or 25 min, during which the bacteria received ES, they were gently washed off the sample electrode surfaces using PBS (pH ~ 7.4) into a sterilized Petri dish. In the following, 10 μL of the washed bacterial

suspension was pipetted onto certain wells of a 96-well plate (already filled with 100 μL of MHB) for the OD_{620} measurement. In parallel, to appear the colony-forming units of the bacteria, another 10 μL of the suspensions were spread gently and uniformly on the surface of the solid agar plates. To further differentiate between the TENG-based and the inherent antibacterial properties of the host materials (*i.e.*, GO or Al), after undergoing ESs, the bacteria were kept exposed to the host electrodes for a longer period (overnight) without further triboelectric effect. To this end, molten agar (~43 °C) was decanted over the host electrodes (already inoculated with bacteria and received treatments) inside the sterilized Petri dishes and allowed to form solid agar. All of the samples were transferred to an incubator (37 °C) and stored overnight.

4.6. Investigation of Live/Dead bacterial staining

Differentiation between damaged/dead and live bacteria was carried out through fluorescent staining according to previous literature [51]. In this investigation, the ES-treated and untreated bacteria were washed off the sample electrodes and then centrifuged at ~ 5 °C and 7000 rpm for 20 min. The obtained bacterial plates were then resuspended in PBS and stained by a mixture of AO/PI fluorescent dyes for 10 min at 37 °C. The samples were subjected to centrifugation (7500 rpm and 5 °C for 7 min) to eliminate the unbonded molecular dyes in the supernatant and extract the dye-bonded bacteria in the sediment. To prepare the samples, 10 μL of the stained bacteria, resuspended in PBS was evenly spread onto clean glass slides. Subsequently, the samples were visualized by using a charge-coupled device (CCD) camera-equipped fluorescence microscope (Zeiss, Germany). In this study, the green and red emissions indicate live and dead bacteria, respectively.

4.7. FE-SEM analysis of bacterial Microstructures

Microstructures of bacteria exposed to electrode samples either in the absence or presence of electrical stimulation were investigated. After incubating the bacteria on the sample electrodes in the same condition applied for antibacterial tests, the bacteria were washed off the electrodes (through 1 mL of PBS) and then centrifuged at ~ 5 °C and 500 rpm. The supernatant was removed and the sedimented bacteria were gently resuspended in PBS and thoroughly spread on clean glass slides (washed with detergent in an ultrasonic bath then rinsed with DI water and ethanol). The bacteria then were fixed for ~ 4 h on the glass slice surface by using 2.5 % glutaraldehyde (glutaraldehyde (25 %): PBS: DI water, 1:4:5) followed by serially dehydration treatments by using orderly aqueous ethanol of 30, 50, 70, 90 and 100 %. The samples were prepared via gold coating for FE-SEM investigations utilizing a MIRA3 TESCAN microscope (Brno, Czech Republic).

4.8. Investigation of in vitro ROS generation

To study the in *vitro* generation of ROS in the bacterial models, two main qualitative and quantitative methods were adopted. In the former method, the generated ROS was visualized by reacting with dichlorofluorescein-diacetate (DCFH-DA), emitting a strong fluorescent green colour due to producing its oxidized form (2′, 7′ dichlorofluorescein (DCF)) [52]. To conduct this study, after exposure to the sample electrode and undergoing the treatment (either in the absence or presence of electrical stimulation), bacterial models were washed off the surfaces and centrifuged at ~ 5 °C and 8000 rpm for 6 min. Afterward, DCFH-DA dye (10×10^{-6} M) was exposed to the harvested bacteria (already redispersed in PBS for 15 min) followed by dropping the samples on clean glass slides. Finally, green fluorescent emission was monitored by exciting the sample (at the wavelength of 488 nm) employing a fluorescent microscope (Zeiss, Germany) equipped with a charge-coupled device (CCD) camera.

To study quantitative in vitro ROS generation in response to finger-tapping electrical stimulation, molecular probes of 1,3-diphenylisobenzofuran (DPBF) and terephthalic acid (TA) as ROS indicators were employed. These indicators exclusively react with specific kinds of ROS of singlet oxygen ($^1O_2$) and hydroxyl radical (OH), respectively. Upon reaction with $^1O_2$, the strong photoluminescent (PL) emission of DPBF at ~ 490 nm drops [53], while after exposure to OH radicals, the non-fluorescent TA is oxidized to 2-hydroxy terephthalic acid (TAOH) emanating a PL peak at ~ 448 nm [33].

4.9. Statistical analysis

The data underwent statistical analysis using the SPSS software package (version 26; SPSS, Inc., Chicago, IL, USA). One-way analysis of variance (ANOVA) was employed with a confidence level set at 99 % and 95 % ($p < 0.01$ and $p < 0.05$, respectively) for determining statistical significance. All data are expressed as mean ± standard deviation based on a minimum of three tests.

CRediT authorship contribution statement

Marziyeh Jannesari: Writing – review & editing, Writing – original draft, Validation, Supervision, Project administration, Methodology, Investigation, Conceptualization. **Faezeh Ejehi:** Writing – review & editing, Writing – original draft, Validation, Supervision, Project administration, Methodology, Investigation, Conceptualization. **Niall J. English:** Writing – review & editing, Writing – original draft, Validation, Supervision, Project administration, Methodology, Investigation, Conceptualization. **Raheleh Mohammadpour:** Writing – review & editing, Writing – original draft, Validation, Supervision, Project administration, Methodology, Investigation, Conceptualization. **Omid Akhavan:** Writing – review & editing, Writing – original draft, Validation, Supervision, Methodology, Investigation, Conceptualization. **Soroush Shams:** Methodology.

Declaration of competing interest

The authors declare that they have no known competing financial interests or personal relationships that could have appeared to influence the work reported in this paper.

Data availability

Data will be made available on request.

Appendix A. Supplementary data

Supplementary data to this article can be found online at https://doi.org/10.1016/j.cej.2024.150036.

References

[1] H. Zheng, Z. Ji, K.R. Roy, M. Gao, Y. Pan, X. Cai, L. Wang, W. Li, C.H. Chang, C. Kaweeteerawat, Engineered graphene oxide nanocomposite capable of preventing the evolution of antimicrobial resistance, ACS Nano 13 (10) (2019) 11488–11499, https://doi.org/10.1021/acsnano.9b04970.
[2] J. Parsonnet, Bacterial infection as a cause of cancer, Environ. Health Perspect. 103 (Suppl 8) (1995) 263–268, https://doi.org/10.1289/ehp.95103s8263.
[3] A. Hogan, V.G. Heppert, A.J. Suda, Osteomyelitis, Arch. Orthop. Trauma Surg. 133 (2013) 1183–1196, https://doi.org/10.1007/s00402-013-1785-7.
[4] C.J. Mathews, V.C. Weston, A. Jones, M. Field, G. Coakley, Bacterial septic arthritis in adults, Lancet 375 (9717) (2010) 846–855, https://doi.org/10.1016/S0140-6736(09)61595-6.
[5] I.N. Okeke, A. Lamikanra, R. Edelman, Socioeconomic and behavioral factors leading to acquired bacterial resistance to antibiotics in developing countries, Emerg. Infect. Dis. 5 (1) (1999) 18, https://doi.org/10.3201/eid0501.990103.
[6] M. Jannesari, J. Varshosaz, M. Morshed, M. Zamani, Composite poly (vinyl alcohol)/poly (vinyl acetate) electrospun nanofibrous mats as a novel wound dressing matrix for controlled release of drugs, Int. J. Nanomedicine (2011) 993–1003, https://doi.org/10.2147/IJN.S17595.
[7] X.F. Wang, M.L. Li, Q.Q. Fang, W.Y. Zhao, D. Lou, Y.Y. Hu, J. Chen, X.Z. Wang, W. Q. Tan, Flexible electrical stimulation device with chitosan-Vaseline(R) dressing

accelerates wound healing in diabetes, Bioact. Mater. 6 (1) (2021) 230–243, https://doi.org/10.1016/j.bioactmat.2020.08.003.
[8] C. Shuai, G. Liu, Y. Yang, F. Qi, S. Peng, W. Yang, C. He, G. Wang, G. Qian, A strawberry-like ag-decorated barium titanate enhances piezoelectric and antibacterial activities of polymer scaffold, Nano Energy 74 (2020) 104825, https://doi.org/10.1016/j.nanoen.2020.104825.
[9] M. Jannesari, E. Asadian, F. Ejehi, N.J. English, R. Mohammadpour, P. Sasanpour, Boosting on-demand antibacterial activity using electrical stimulations from polypyrrole-graphene oxide triboelectric nanogenerator, Nano Energy 112 (2023) 108463, https://doi.org/10.1016/j.nanoen.2023.108463.
[10] G.Q. Gu, C.B. Han, J.J. Tian, C.X. Lu, C. He, T. Jiang, Z. Li, Z.L. Wang, Antibacterial composite film-based triboelectric nanogenerator for harvesting walking energy, ACS Appl. Mater. Interfaces. 9 (13) (2017) 11882–11888, https://doi.org/10.1021/acsami.7b00230.
[11] X. Peng, K. Dong, C. Ye, Y. Jiang, S. Zhai, R. Cheng, D. Liu, X. Gao, J. Wang, Z.L. Wang, A breathable, biodegradable, antibacterial, and self-powered electronic skin based on all-nanofiber triboelectric nanogenerators, Sci. Adv., 6 (26), 2020, eaba9624, 10.1126/sciadv.aba9624.
[12] F. Ejehi, R. Mohammadpour, E. Asadian, S. Fardindoost, P. Sasanpour, Enhancement of self-powered humidity sensing of graphene oxide–based triboelectric nanogenerators by addition of graphene oxide nanoribbons, Mikrochim. Acta 188 (2021) 1–13, https://doi.org/10.1038/s41598-020-64490-7.
[13] S. Cui, Y. Zheng, J. Liang, D. Wang, Conducting polymer PPy nanowire-based triboelectric nanogenerator and its application for self-powered electrochemical cathodic protection, Chem. Sci. 7 (10) (2016) 6477–6483, https://doi.org/10.1039/C6SC02562E.
[14] Y. Kim, D. Lee, J. Seong, B. Bak, U.H. Choi, J. Kim, Ionic liquid-based molecular design for transparent, flexible, and fire-retardant triboelectric nanogenerator (TENG) for wearable energy solutions, Nano Energy 84 (2021) 105925, https://doi.org/10.1016/j.nanoen.2021.105925.
[15] F. Ejehi, R. Mohammadpour, E. Asadian, P. Sasanpour, S. Fardindoost, O. Akhavan, Graphene oxide papers in nanogenerators for self-powered humidity sensing by finger tapping, Sci. Rep. 10 (1) (2020) 7312, https://doi.org/10.1038/s41598-020-64490-7.
[16] J. Zhang, X. Zhao, Z. Wang, Z. Liu, S. Yao, L. Li, Antibacterial, antifreezing, stretchable, and self-healing organohydrogel electrode based triboelectric nanogenerator for self-powered biomechanical sensing, Adv. Mater. Interfaces 9 (15) (2022) 2200290, https://doi.org/10.1002/admi.202200290.
[17] Y. Jiang, K. Dong, J. An, F. Liang, J. Yi, X. Peng, C. Ning, C. Ye, Z.L. Wang, UV-protective, self-cleaning, and antibacterial nanofiber-based triboelectric nanogenerators for self-powered human motion monitoring, ACS Appl. Mater. Interfaces. 13 (9) (2021) 11205–11214, https://doi.org/10.1021/acsami.0c22670.
[18] W. Zhang, Y. Zhang, G. Yang, X. Hao, X. Lv, F. Wu, J. Liu, Y. Zhang, Wearable and self-powered sensors made by triboelectric nanogenerators assembled from antibacterial bromobutyl rubber, Nano Energy 82 (2021) 105769, https://doi.org/10.1016/j.nanoen.2021.105769.
[19] Y. Lu, H. Xiang, Y. Jie, X. Cao, Z.L. Wang, Antibacterial triboelectric nanogenerator for mite removal and intelligent human monitoring, Adv. Mater. Technol. 2300192 (2023), https://doi.org/10.1002/admt.202300192.
[20] I.C. Candido, G.d.S. Oliveira, G.G. Viana, F.A.G. da Silva Jr, M.M. da Costa, H.P. de Oliveira, Wearable triboelectric nanogenerators based on chemical modification of conventional textiles for application in electrically driven antibacterial devices, ACS Appl. Electron. Mater. 4 (1) (2021) 334–344, https://doi.org/10.1021/acsaelm.1c01028.
[21] H.Y. Mao, S. Laurent, W. Chen, O. Akhavan, M. Imani, A.A. Ashkarran, M. Mahmoudi, Graphene: promises, facts, opportunities, and challenges in nanomedicine, Chem. Rev. 113 (5) (2013) 3407–3424, https://doi.org/10.1021/cr300335p.
[22] C. Zhu, T.-Y.-J. Han, E.B. Duoss, A.M. Golobic, J.D. Kuntz, C.M. Spadaccini, M. A. Worsley, Highly compressible 3D periodic graphene aerogel microlattices, Nat. Commun. 6 (1) (2015) 6962, https://doi.org/10.1038/ncomms7962.
[23] S. Taghipour, M. Jannesari, M. Taghipour, B. Ataie-Ashtiani, O. Akhavan, Synthesis and application of carbon-based nanomaterials for bioelectrochemical systems, Advanced Nanomaterials and Nanocomposites for Bioelectrochemical Systems, Elsevier2023, pp. 327-356.
[24] K.I. Bolotin, K. Sikes, Z. Jiang, M. Klima, G. Fudenberg, J. Hone, P. Kim, H. L. Stormer, Ultrahigh electron mobility in suspended graphene, Solid State Commun. 146 (9–10) (2008) 351–355, https://doi.org/10.1016/j.ssc.2008.02.024.
[25] O. Akhavan, M. Saadati, M. Jannesari, Graphene jet nanomotors in remote controllable self-propulsion swimmers in pure water, Nano Lett. 16 (9) (2016) 5619–5630, https://doi.org/10.1021/acs.nanolett.6b02175.
[26] O. Akhavan, Graphene nanomesh by ZnO nanorod photocatalysts, ACS Nano 4 (7) (2010) 4174–4180, https://doi.org/10.1021/nn1007429.
[27] M. Jannesari, O. Akhavan, H.R.M. Hosseini, Graphene oxide in generation of nanobubbles using controllable microvortices of jet flows, Carbon 138 (2018) 8–17, https://doi.org/10.1016/j.carbon.2018.05.068.
[28] R. Zhang, M. Hummelgård, J. Örtegren, H. Andersson, M. Olsen, D. Chen, J. Li, A. Eivazi, C. Dahlström, M. Norgren, Triboelectric nanogenerators with ultrahigh current density enhanced by hydrogen bonding between nylon and graphene oxide, Nano Energy 115 (2023) 108737.
[29] M. Lamberti, F. Escher, Aluminium foil as a food packaging material in comparison with other materials, Food Rev. Intl. 23 (4) (2007) 407–433.
[30] O. Akhavan, The effect of heat treatment on formation of graphene thin films from graphene oxide nanosheets, Carbon 48 (2) (2010) 509–519, https://doi.org/10.1016/j.carbon.2009.09.069.
[31] O. Akhavan, K. Bijanzad, A. Mirsepah, Synthesis of graphene from natural and industrial carbonaceous wastes, RSC Adv. 4 (39) (2014) 20441–20448, https://doi.org/10.1039/C4RA01550A.
[32] L. Stobinski, B. Lesiak, A. Malolepszy, M. Mazurkiewicz, B. Mierzwa, J. Zemek, P. Jiricek, I. Bieloshapka, Graphene oxide and reduced graphene oxide studied by the XRD, TEM and electron spectroscopy methods, J. Electron Spectrosc. Relat. Phenom. 195 (2014) 145–154.
[33] M. Jannesari O. Akhavan H.R. Madaah Hosseini B. Bakhshi Graphene/CuO2 nanoshuttles with controllable release of oxygen nanobubbles promoting interruption of bacterial respiration ACS Appl. Mater. Interfaces. 12 32 2020 35813 35825 10.1021/acsami.0c05732.
[34] D. Graf, F. Molitor, K. Ensslin, C. Stampfer, A. Jungen, C. Hierold, L. Wirtz, Spatially resolved raman spectroscopy of single-and few-layer graphene, Nano Lett. 7 (2) (2007) 238–242, https://doi.org/10.1021/nl061702a.
[35] F.L. Hirshfeld, Bonded-atom fragments for describing molecular charge densities, Theor. Chim. Acta 44 (1977) 129–138, https://doi.org/10.1007/BF00549096.
[36] M.D. Rolfe, C.J. Rice, S. Lucchini, C. Pin, A. Thompson, A.D. Cameron, M. Alston, M.F. Stringer, R.P. Betts, J. Baranyi, Lag phase is a distinct growth phase that prepares bacteria for exponential growth and involves transient metal accumulation, J. Bacteriol. 194 (3) (2012) 686–701.
[37] O. Akhavan, E. Ghaderi, Escherichia coli bacteria reduce graphene oxide to bactericidal graphene in a self-limiting manner, Carbon 50 (5) (2012) 1853–1860, https://doi.org/10.1016/j.carbon.2011.12.035.
[38] N. Saadi, K. Alotaibi, L. Hassan, Q. Smith, F. Watanabe, A.A. Khan, T. Karabacak, Enhancing the antibacterial efficacy of aluminum foil by nanostructuring its surface using hot water treatment, Nanotechnology 32 (32) (2021) 325103.
[39] A.R. Aref, M. Campisi, E. Ivanova, A. Portell, D. Larios, B.P. Piel, N. Mathur, C. Zhou, R.V. Coakley, A. Bartels, 3D microfluidic ex vivo culture of organotypic tumor spheroids to model immune checkpoint blockade, Lab Chip 18 (20) (2018) 3129–3143, https://doi.org/10.1039/C8LC00322J.
[40] M. Jannesari, O. Akhavan, H.R.M. Hosseini, B. Bakhshi, Oxygen-rich graphene/ZnO_2-ag nanoframeworks with pH-switchable catalase/peroxidase activity as O_2 nanobubble-self generator for bacterial inactivation, J. Colloid Interface Sci. 637 (2023) 237–250, https://doi.org/10.1016/j.jcis.2023.01.079.
[41] C. Weng, L. Shen, J.W. Teo, Z.C. Lim, B.S. Loh, W.H. Ang, Targeted antibacterial strategy based on reactive oxygen species generated from dioxygen reduction using an organoruthenium complex, JACS Au 1 (9) (2021) 1348–1354, https://doi.org/10.1021/jacsau.1c00262.
[42] D.R. Lovley, Happy together: microbial communities that hook up to swap electrons, ISME J. 11 (2) (2017) 327–336, https://doi.org/10.1038/ismej.2016.136.
[43] Y. Anraku, Bacterial electron transport chains, Annu. Rev. Biochem 57 (1) (1988) 101–132, https://doi.org/10.1146/annurev.bi.57.070188.000533.
[44] V.R. Kaila, M. Wikström, Architecture of bacterial respiratory chains, Nat. Rev. Microbiol. 19 (5) (2021) 319–330, https://doi.org/10.1038/s41579-020-00486-4.
[45] M. Jastroch, A.S. Divakaruni, S. Mookerjee, J.R. Treberg, M.D. Brand, Mitochondrial proton and electron leaks, Essays Biochem. 47 (2010) 53–67, https://doi.org/10.1042/bse0470053.
[46] E.C. Salas, Z. Sun, A. Lüttge, J.M. Tour, Reduction of graphene oxide via bacterial respiration, ACS Nano 4 (8) (2010) 4852–4856, https://doi.org/10.1021/nn101081t.
[47] G. Cecchini, Function and structure of complex II of the respiratory chain, Annu. Rev. Biochem 72 (1) (2003) 77–109, https://doi.org/10.1146/annurev.biochem.72.121801.161700.
[48] J.P. Perdew, K. Burke, M. Ernzerhof, Generalized gradient approximation made simple, Phys. Rev. Lett. 77 (18) (1996) 3865, https://doi.org/10.1103/PhysRevLett.77.3865.
[49] S. Zhou, S. Kim, A. Bongiorno, Chemical structure of oxidized multilayer epitaxial graphene: a density functional theory study, J. Phys. Chem. C 117 (12) (2013) 6267–6274, https://doi.org/10.1021/jp400128t.
[50] Z. Futera, N.J. English, Communication: Influence of external static and alternating electric fields on water from long-time non-equilibrium ab initio molecular dynamics, J. Chem. Phys, 147 (3), 2017, 10.1063/1.4994694.
[51] Y. Liu, J. Wen, Y. Gao, T. Li, H. Wang, H. Yan, B. Niu, R. Guo, Antibacterial graphene oxide coatings on polymer substrate, Appl. Surf. Sci. 436 (2018) 624–630, https://doi.org/10.1016/j.apsusc.2017.12.006.
[52] S. Panda, T.K. Rout, A.D. Prusty, P.M. Ajayan, S. Nayak, Electron transfer directed antibacterial properties of graphene oxide on metals, Adv. Mater. 30 (7) (2018) 1702149, https://doi.org/10.1002/adma.201702149.
[53] A.M. Asadirad, Z. Erno, N.R. Branda, Photothermal release of singlet oxygen from gold nanoparticles, Chem. Commun. 49 (50) (2013) 5639–5641, https://doi.org/10.1039/C3CC42217H.